TRAVERSING THE SUBSPACE OF ADVERSARIAL PATCHES

Jens Bayer

Fraunhofer Center for Machine Learning, Fraunhofer IOSB Gutleuthausstr. 1, Ettlingen, Germany jens.bayer@iosb.fraunhofer.de

Stefan Becker

Fraunhofer IOSB Gutleuthausstr. 1, Ettlingen, Germany

David Münch

Fraunhofer IOSB Gutleuthausstr. 1, Ettlingen, Germany

Michael Arens

Fraunhofer IOSB Gutleuthausstr. 1, Ettlingen, Germany

Jürgen Beyerer

Karlsruher Institute of Technology, Fraunhofer Center for Machine Learning, Fraunhofer IOSB Fraunhoferstr. 1, Karlsruhe, Germany

December 3, 2024

ABSTRACT

Despite ongoing research on the topic of adversarial examples in deep learning for computer vision, some fundamentals of the nature of these attacks remain unclear. As the manifold hypothesis posits, high-dimensional data tends to be part of a low-dimensional manifold. To verify the thesis with adversarial patches, this paper provides an analysis of a set of adversarial patches and investigates the reconstruction abilities of three different dimensionality reduction methods. Quantitatively, the performance of reconstructed patches in an attack setting is measured and the impact of sampled patches from the latent space during adversarial training is investigated. The evaluation is performed on two publicly available datasets for person detection. The results indicate that more sophisticated dimensionality reduction methods offer no advantages over a simple principal component analysis.

Keywords Adversarial Attacks, Manifold Learning, Object Detection

1 Introduction

Adversarial patch attacks in deep learning for computer vision are a quite well-known topic, yet, some fundamentals of the nature of these powerful attacks remain unclear. Due to the complexity of deep neural networks, where these patches are optimized on, there are no straightforward explanations why a generated pattern, looks the way it does. Moreover, there are no explainability methods like those used for deep neural networks that provide a human-understandable explanation of why these patches prevent a network from working properly. To further understand these high-dimensional data, this paper follows the manifold hypothesis [1]. For adversarial attacks, this states, that adversarial patterns are part of a lower-dimensional manifold. This paper builds on our recently published work "Eigenpatches – Adversarial Patches from Principal Components" [2]. By applying a principal component analysis (PCA) on a set of the trained adversarial patches, it could already be shown that linear combinations of Eigenpatches can be used to successfully attack the investigated YOLOv7 object detector [3].

The contributions of this paper are:

- (i) A more in-depth analysis of a crafted set of adversarial patches.
- (ii) An evaluation of the performance of patches sampled from different low-dimensional manifolds and further analyze their generalization ability by evaluating them across varying detection models and datasets.
- (iii) An evaluation of the impact of the usage of sampled adversarial patches from those manifolds when used in adversarial training.

The structure of the paper is as follows: In Section 2 the similarities and distinctions between related work and this paper are presented. Section 3 covers the fundamentals of eigenpatches and presents the alternative manifold learning methods that are evaluated. The experiments and the results are described in Section 4. A discussion, followed by a brief conclusion and outlook, is given in Section 5.

2 Related work

Despite being an active research area, the focus of analyzing adversarial patterns is rarely [4] on object detector methods and adversarial patches. Instead, the investigations are performed mostly on image classifiers and attacks that induce high-frequent noise across the whole image [5, 6, 7, 8, 9, 10, 11]. Therefore only some selected works on analyzing adversarial attack patterns and sampling from low-dimensional embeddings are presented. For an overview of the different approaches to adversarial attacks, we refer to these surveys [12, 13, 14, 15].

Wang et al. [6] propose a fast black-box adversarial attack that identifies key differences between different classes using a PCA. The principal components are then used to manipulate a sample into either a target class or the nearest other class.

Similarly, yet different, *Energy Attack* from Shi et al. [7] leverages PCA to obtain the energy distribution of perturbations generated by white-box attacks on a surrogate model. This transfer-based black-box adversarial attack samples patches according to the energy distribution, tiles them, and applies them to the target image. The extracted patches are high-frequent noise and are used to attack image classifiers. Despite the name, they should therefore not be confused with adversarial patches that are used to attack object detectors in a physical world attack.

Another approach uses the singular value decomposition and is presented by Weng et al. [10]. The authors combine the top-1 decomposed singular value-associated features for computing the output logits with the original logits, used to optimize adversarial examples. This results in an improvement in the transferability of the attacks.

Regarding the subspace of adversarial examples, researches have explored methods to estimate the dimensionality of the space of adversarial inputs.

Dohmatob et al. [8], for example, investigate the vulnerability of neural networks to black-box attacks, specifically examining low-dimensional adversarial perturbations. They found that adversarial perturbations are likely to exist in low-dimensional subspaces that are much smaller than the dimension of the image space, supporting the manifold hypothesis.

An explicit estimation of the dimensionality of shared adversarial subspaces of, e.g., two fully connected networks trained on two different datasets, is presented in [5]. By examining untargeted misclassification attacks they demonstrate that manipulating a data point to cross a model's decision boundary is likely to result in similar performance degradation when applied to other models.

Tarchoun et al. [4] recently studied adversarial patches from an information theory perspective, measuring the entropy of random crops of the patches. Their findings indicate that the mean entropy of adversarial patches is higher than in natural images. Based on these results, they developed a defense mechanism against adversarial patches.

Moreover, theoretical limits on the susceptibility of classifiers to adversarial attacks are demonstrated by Shafahi et al. [9] using a unit sphere and unit cube. They suggest that these bounds may be potentially bypassed by employing extremely large values for the class densitiy functions. Furthermore, their findings suggest that the fundamental limits of adversarial training for specific datasets with complex image classes in high-dimensional spaces are far worse than one expects.

Godfrey et al. [16] conducted further research on the relationship between adversarial vulnerability and the number of perturbed dimensions. Their findings support the hypothesis that adversarial examples are a result of the locally linear behavior of neural networks with high-dimensional input spaces.

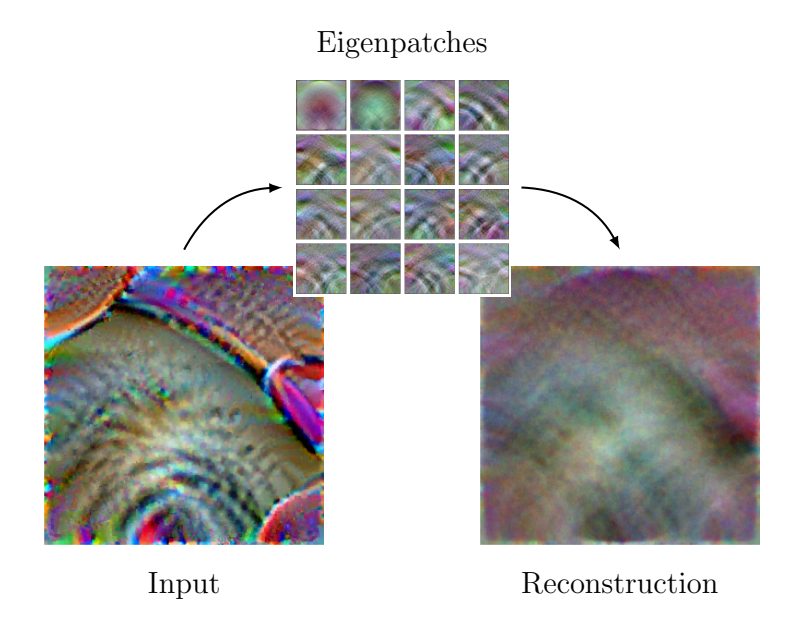


Figure 1: Reconstruction (right) of an adversarial patch (left) using the first 16 Eigenpatches (middle) [2].

While the related works mainly focus on adversarial examples for image classifiers, this work explores commonalities of adversarial patch attacks against object detectors. The investigated dimensionality reduction methods are evaluated in an attack setting and also tested if sampled patches can be used in adversarial training.

3 Fundamentals

The following section covers the necessary theoretical backgrounds of the investigated dimensionality reduction methods and manifold learning techniques. To be more precise, Eigenpatches and autoencoders are investigated. Both methods offer an embedding of the data in a low-dimensional space while also providing a simple sampling strategy.

3.1 Eigenpatches

Eigenpatches or Eigenimages [17] are calculated on a set of adversarial patches [2]. The term Eigenimages is the name of the eigenvectors that can be derived from a set of training images when a PCA is applied. In general, Eigenimages can be used to represent the original training images and recreate these through a linear combination of the low-dimensional representation.

Given a set of adversarial patches

$$\mathcal{P} = \{ \mathbf{P}_i | i = 1, \dots, n \}, \quad \mathbf{P}_i \in [0, 1]^{C \times H \times W}$$

$$\tag{1}$$

where H is the height in pixel, W is the width in pixel and C is the number of channels. A principal component analysis is performed on \mathcal{P} . With the top k principal components $\mathbf{E}_j, j \in \{1, \dots, k\}$ and the weights $\lambda_{i,j}$, the set

$$\hat{\mathcal{P}} = \{\hat{\mathbf{P}}_i | i = 1, \dots, n\} \quad \hat{\mathbf{P}}_i = \sum_{j=1}^k \lambda_{i,j} \mathbf{E}_j$$
(2)

can be generated that consists of linear combinations of the principal components and is a recreation of \mathcal{P} [2].

In some cases, especially when the data lies on or near a low-dimensional manifold within the high-dimensional space, a PCA can be considered a way to approximate that manifold. However, a PCA does not explicitly model the manifold structure of the data. It operates under the assumption, that the principal components capture the most important directions in the data, but it doesn't take into account the non-linear relationships or intrinsic geometry that may exist in the data.

To also take non-linearities into account, alternative methods are required. One particular set of manifold learning techniques that are capable of extracting underlying structures from high-dimensional data and projecting these onto a lower-dimensional space are autoencoders.

3.2 Autoencoders

Autoencoders are particularly valuable in manifold learning due to their ability to learn compact and meaningful representations of high-dimensional data [18]. By compressing the data into a lower dimensional latent space, autoencoders effectively capture the essential features and structure of the data manifold. In general, autoencoders first encode the input data and decode them after they were propagated through a bottleneck. During training, the reconstruction loss is utilized to train the network weights. To capture spatial relation within image data, convolutional autoencoders are used, as they replace the fully connected layers with convolutional layers in both the encoder and decoder [18].

An extension that introduces a probabilistic approach on learning the latent space representation are variational autoencoders (VAE). They model the latent space as a probability distribution, allowing for more flexible generation of new data points [19]. In addition to the reconstruction loss, the Kullback-Leibler divergence is calculated and used as a regularization term to encourage the model to not focus on perfect reconstructions but rather be good at creating new data [20].

The experiments described in the next section use a convolutional autoencoder and a conditional variational autoencoder to generate reconstructions of the training data and sample new adversarial patches. The conditional variational autoencoder is a variant of the variational autoencoder that uses additional information during the encoding and decoding to condition the probability distribution [18].

4 Experiments

4.1 Setup

In the following, the experiments and the three different dimensionality reduction methods (see Figure 2) are described and evaluated.

If not stated otherwise, all experiments use the YOLOv7 tiny model as architecture. Furthermore, this paper uses the same patch set as [2]. They are referred as *prime patches* in the following. The prime patches are trained with different combinations (A-E) of rotation, scale and lr-scheduler parameters as described in [2] (see Table 4). They are optimized on the YOLOv7 tiny model with the provided pretrained weights and the *INRIA Person* dataset.

To measure the impact on the performance of the detector, the mean average precision (mAP) is used. The up/down facing arrows (\uparrow/\downarrow) in the tables indicate that a higher/lower score is more desirable. This is particularly important to keep in mind, since a high mAP is desired in the case of adversarial training and a low mAP in the case of a successful reconstruction of a prime patch.

4.1.1 Object Detector

As in [2], YOLOv7 is used as a reference object detector. For the evaluation of adversarial training with patch reconstructions, the same training procedure is used for each trained model. SGD with the default parameters to train the model from scratch provided by the official git repository is used. The batch size is set to 32 and the probability, for a bounding box to contain a patch, is set to $\pi = 0.25$.

The single-patched network is trained with only a single prime patch and has not seen other patches during training. The multi-patched networks are trained with multiple patches and have therefore seen various patches during training. If an image is patched in a multi-patched network, all boxes in the image share the same patch.

The prime multi-patched network is trained with 10 randomly predefined prime patches (see Figure 6).

The PCA multi-patched networks are trained with linear combinations of Eigenpatches. The weights for the linear combination are sampled from normal distributions with means and standard deviations calculated regarding the encoded prime patches.

Patches used in the convolutional autoencoder multi-patched network training are sampled by uniformly selecting a random point in the latent space, bounded by the values of the encoded prime patches.

Similarly, the patches used in the training of the variational autoencoder multi-patched network are sampled. Here, values in the latent space are sampled from the underlying normal distribution, conditioned to a randomly chosen parameter group.

¹https://github.com/WongKinYiu/yolov7

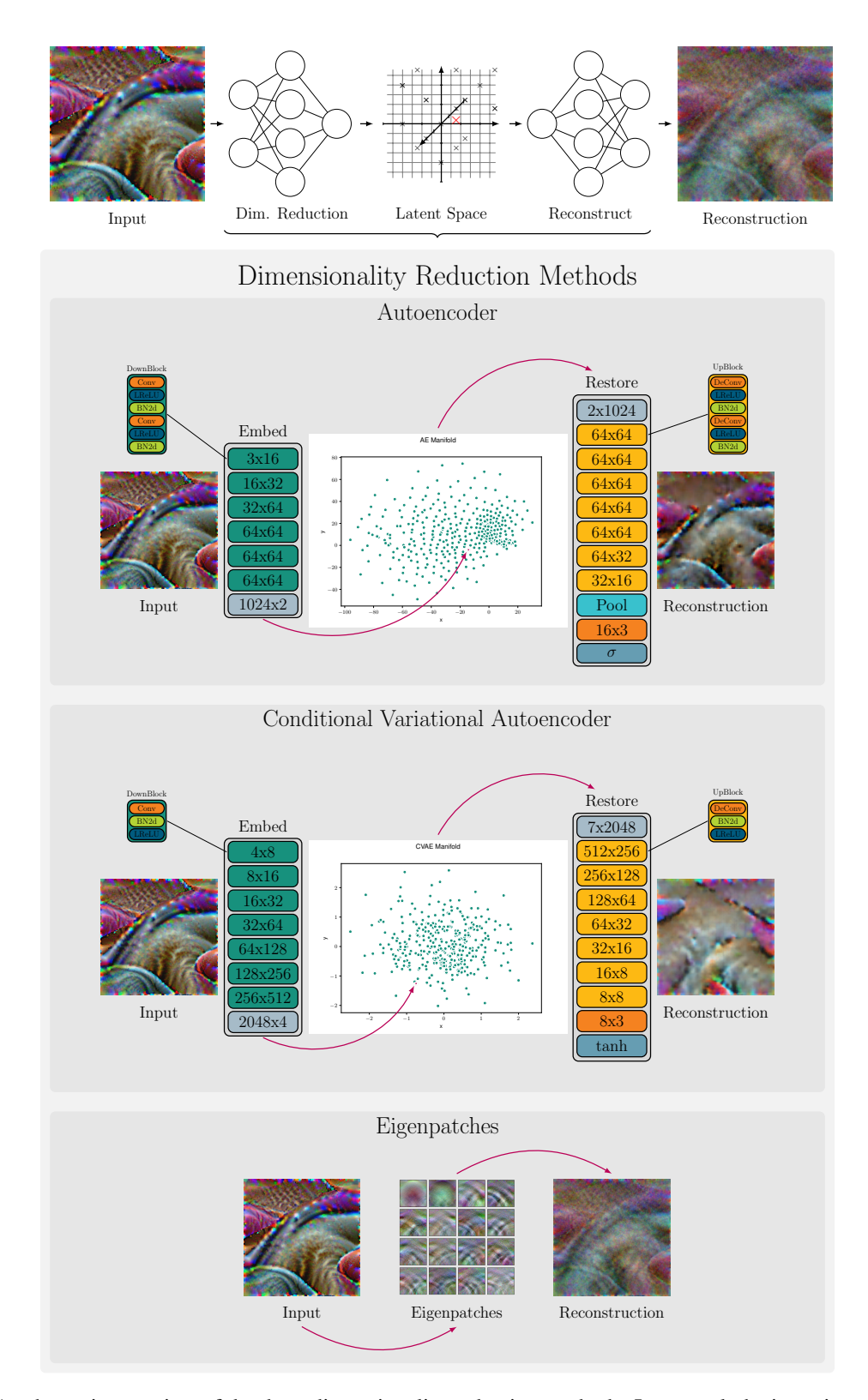


Figure 2: A schematic overview of the three dimensionality reduction methods. In general, the input is a prime patch, which will be encoded by a dimensionality reduction method. Both autoencoder approaches have a latent space with two dimensions. The number of dimensions for the PCA depends on the chosen number of principal components and varies between 16, 32, 64, and 128 dimensions. Based on the encoding in the latent space, the input is reconstructed.

4.1.2 Datasets

For the experiments, the *INRIA Person* dataset [21] and the *Crowdhuman* dataset [22] are used. Both datasets contain images of persons in various environments.

The INRIA Person dataset is a small dataset where the selected subset contains a total of 585 train images with 3 317 bounding boxes and 288 test images with 904 bounding boxes. The dataset has also been used to generate the prime patches.

To verify the experiments, the Crowdhuman dataset is used, which is a benchmark dataset for person detection. The dataset contains $15\,000$ images in the training set, $4\,370$ in the validation set and $5\,000$ images in the test set. The total number of human instances in all sets is $470\,000$. For our experiments, we use the train set and validation set. Since there are numerous small bounding boxes, each bounding box with less than $4\,096$ pixels is filtered and removed from the dataset. This reduces the number of bounding boxes in the training set from $332\,914$ to $109\,836$ and in the validation set from $97\,529$ to $32\,392$.

4.1.3 Autoencoders

A schematic of the architecture of both autoencoder models can be found in Figure 2. Both models are trained over 2000 epochs on the prime patches with an initial learning rate of 0.01 and the *AdamW* [23] optimizer. Each 100 epochs, the learning rate is reduced by a factor of 10. The batch size for both models is set to 64 and the bottleneck size is set to 2. For both models, the mean squared error between the input and output is optimized. The variational autoencoder also optimizes the KL-Div loss.

4.2 T-Distributed Stochastic Neighbor Embeddings

The prime patches and their influence on the activation of the last convolutional layer of the backbone layer in the YOLOv7 object detector can be seen in Figure 3. The different colors in the plots correspond to the mean average precision the detector achieves after the bounding boxes in the image are attacked with a patch. The bright yellow dot is the activation of the original image without any patches present. The marker symbol of each data point corresponds to the parameter set used to optimize the patch. In addition to the five different prime patch parameter sets, a total number of 100 random noise patches and 100 grayscale patches are also shown.

The first experiment is about the t-distributed stochastic neighbor embeddings (t-SNE) of the prime patches. This set of qualitative experiments provides a more general overview of the impact of the patches on the pretrained object detector.

The embeddings of the patch activations for a single image in Figure 3 show five distinct clusters among the different patches. The original activation of the unpatched image is given by the yellow dot at about (x=30,y=-13). Right next to this dot, the activations of the different grayscale levels form a c-shape. The colors of the data points and the position in the neighborhood of the original activations indicate that the impact of the grayscale patches is low $(mAP=0.79\pm0.02)$.

The second cluster with a relatively high mAP is given by the random patches. The center of this cluster is above the first cluster at around (20, 15). In contrast to the grayscale patches, the random patches have a slightly deeper shade, which indicates that the random noise has a slightly stronger negative impact on the detector than the grayscale patches (0.75 ± 0.01) . At the edge is a single prime patch of the parameter set C.

The remaining data points of parameter set C are mixed with patches of parameter sets A and D in the upper left cluster, with the center at around (-12,25). The shade of the cluster is darker than the shade of the previous two clusters (0.69 ± 0.06) .

Both remaining clusters contain data points of the parameter set B. The cluster at (-35, 5) is a pure cluster of data points from parameter set B and is much denser compared to the remaining one. Both clusters have similar mAP of 0.63 ± 0.08 and 0.63 ± 0.05 , yet the last remaining cluster with the center at around (-10, -10) contains the data points with the lowest mAP values.

These observations demonstrate that noise and grayscale patches have almost no impact on the object detector on this specific input image. Furthermore, patches that share an optimization parameter set alter the backbone activations similarly.

As this form of representation only shows the impact of a patch on a single image, another representation is given in Figure 4. Here, each data point of the t-SNE plot corresponds to the patch itself. The colors of the data points in this

Prime Patches Backbone Activations

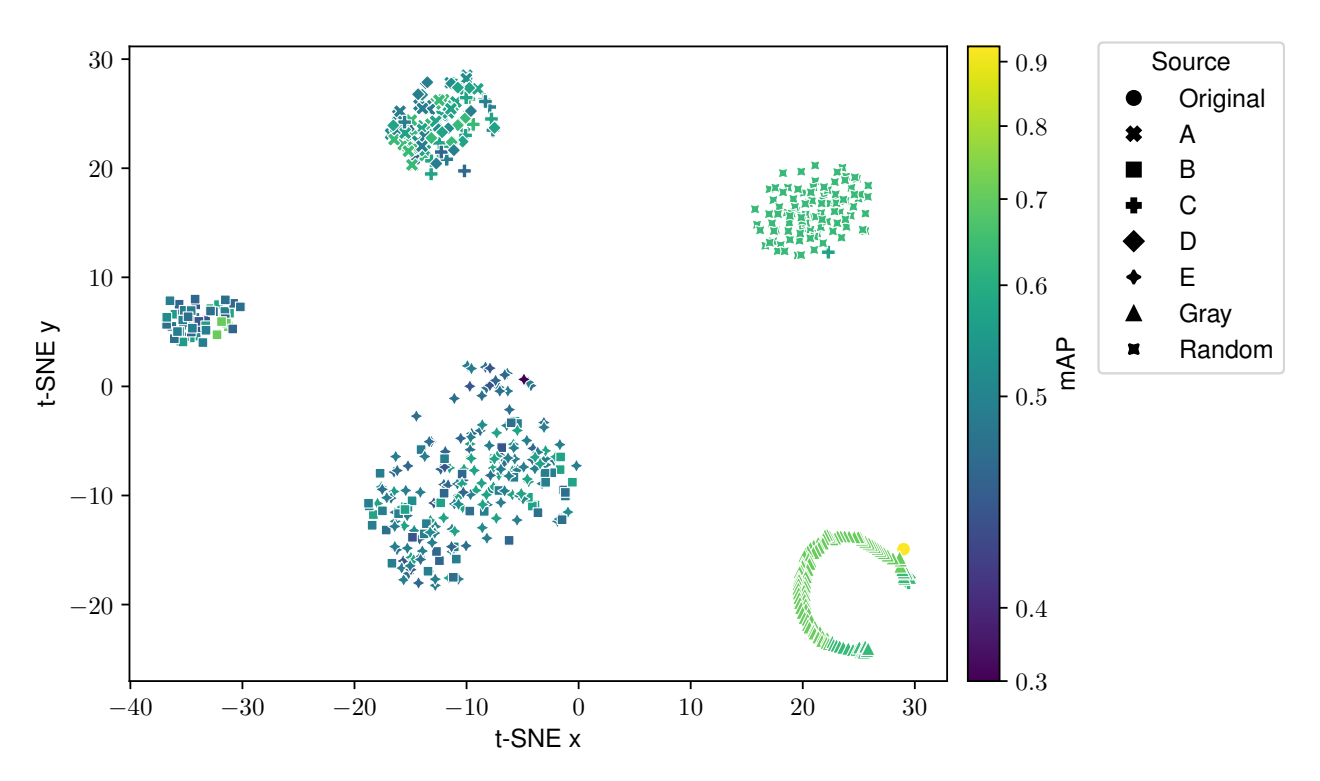


Figure 3: t-SNE plot of the model backbone activation when attacked with a certain patch. Each marker represents a single patch, embedded at the same position in the same image. The color indicates the impact of the patch on the mean average precision. The parameter set of the patch is given by its marker symbol. The plot includes the prime patches, 100 random sampled patches as well as 100 grayscale patches. The parameter settings (A-E) used to train a certain prime patch correspond to the parameters presented in [2].

plot encode the overall mean average precision drop in detection performance for the *INRIA Person* test set. Again, the marker symbol corresponds to the parameter set used to optimize the prime patch.

4.3 Attack Performance

The next experiment covers the attack performance on the pretrained object detector when reconstructed patches are used. In Figure 5, the data points correspond to reconstructions of prime patches and prime patches themselves. Again, the color encodes the mAP value of the corresponding patch. The marker symbol, on the other hand, provides information about the used dimensionality reduction method.

CVAE is the conditional variational autoencoder. As the positions of the markers indicate, the method fails the reconstruction of the patches in most cases. Instead, multiple patches are alike. The mean Euclidean distance of the embedded CVAE patches to its corresponding prime embedding is 36.81 ± 29.31 and the highest among all three investigated methods.

The embeddings of the auto encoder reconstructions (AE) are more scattered and less focused on a few spots. The mean Euclidean distance of 5.27 ± 8.58 supports this.

The method with the lowest mean Euclidean distance of 2.96 ± 7.10 is the PCA with 64 components. As shown in the plot, most prime patches can be sufficiently reconstructed. Only the patches of parameter set E seem more challenging.

Regarding the performance of the reconstructed patches in an attack setting, all three methods are able to reconstruct patches that result in a mean decline of the detector performance by more than 0.2 (see Table 1). The prime patches and grayscale patches in the table can be considered an upper and lower bound for the patch performance.

t-SNE Prime Patch Embedding

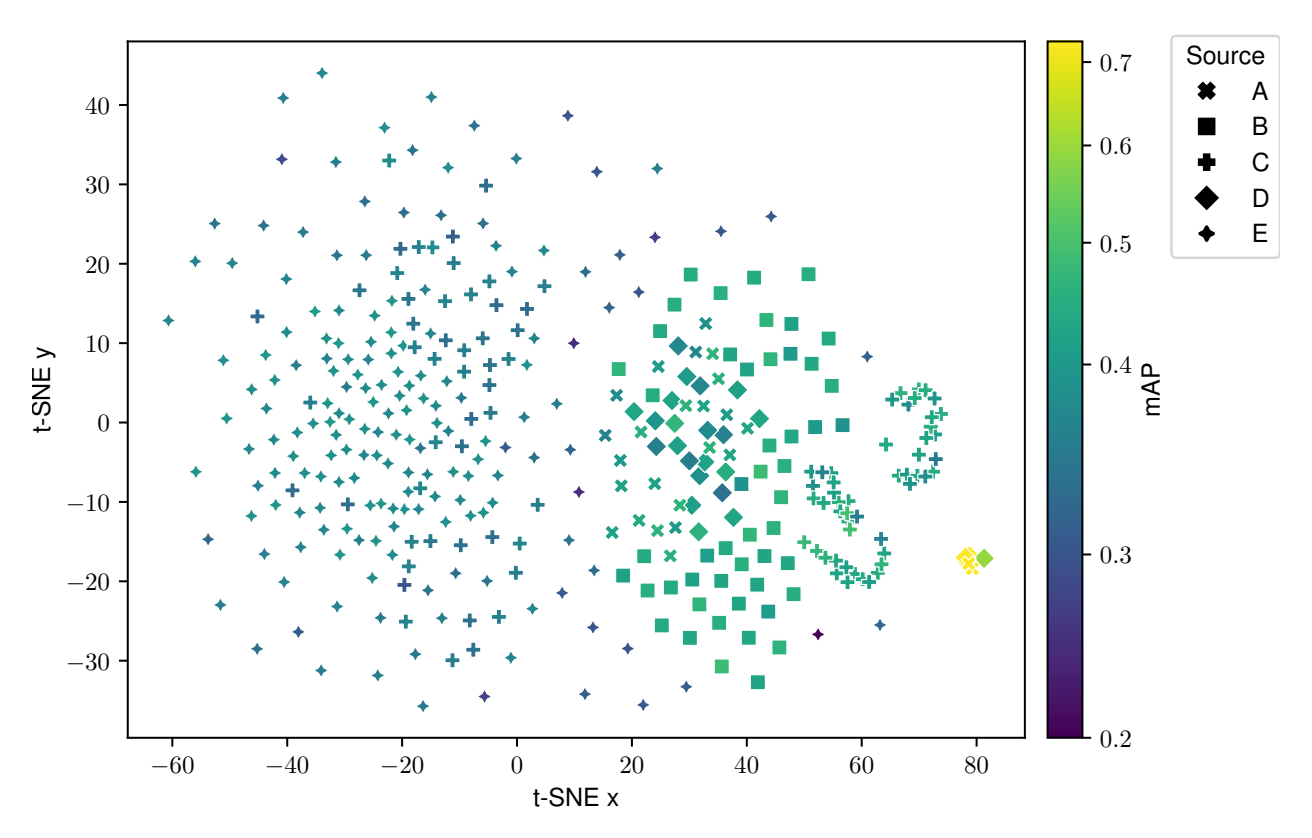


Figure 4: t-SNE plot of the pixel values of each prime patch. The color indicates the impact of the patch on the mean average precision measured with the *INRIA Person* test set. The parameter set of a patch is given by its marker symbol.

Table 1: Mean average precision of the COCO-pretrained YOLOv7 tiny model, on the *INRIA Person* test set. The patch mode indicates, which patches are used during the attack: None is the default without any patches. Grayscale are different grayscale levels.

Patch Mode	n	mAP 0.5 ↓	mAP 0.5:0.95↓
None	1	0.96	0.90
Grayscale	11	0.84 ± 0.02	0.71 ± 0.01
Prime Patches	375	0.57 ± 0.06	0.39 ± 0.06
PCA (64)	375	0.70 ± 0.04	0.54 ± 0.04
AE	375	0.73 ± 0.04	0.55 ± 0.05
CVAE	375	0.72 ± 0.04	$\boldsymbol{0.53 \pm 0.05}$

4.4 Adversarial Training

Table 2 and Table 3 show the results of the adversarial training. Each row represents a trained network. The patch mode indicates, which method was used to provide the adversarial patches during training. *None* is the trained network without any adversarial patches present during training.

In Table 2, the problem with training on a small data basis as the selected subset of the *INRIA Person* dataset becomes visible. The induced adversarial patches during training can be considered as a form of data augmentation, resulting in a higher overall mAP. Interestingly, the networks are prone to grayscale patches, while at the same time, have learned to ignore or rather profit from adversarial patches on bounding boxes of interest. A possible fix could be to include grayscale patches during training.

t-SNE Reconstructed Patches Embeddings

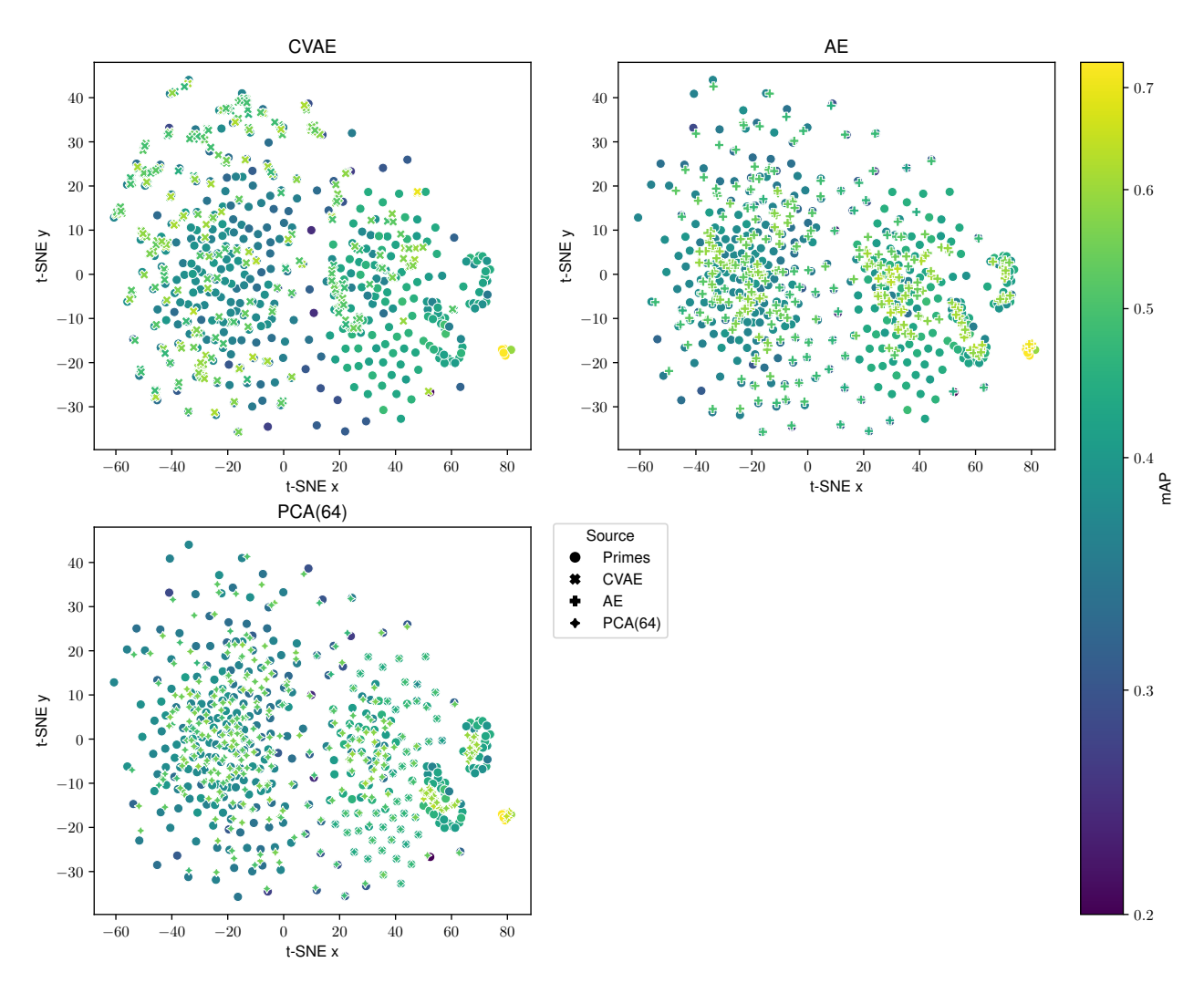


Figure 5: t-SNE plots of the three reconstruction methods. Conditional Variational Autoencoder (CVAE), Autoencoder (AE) and Principal Component Analysis with 64 components (PCA(64)). Again, the color indicates the impact on the mean average precision measured with the *INRIA Person* test set. The marker symbol shows, whether it is a reconstruction from the corresponding construction method or a prime patch.

The highest mAP when attacked with prime patches achieves the PCA (128) network. The best performance without any patches visible has the PCA (16) network. The PCA (64) network has the highest mAP when grayscale patches are visible.

When trained on the Crowdhuman dataset, the results are as expected (see Table 3): The induced adversarial patches during training affect the network performance when no patches are present, and further improve the performance when patches are present. The latter finding supports the thesis that adversarial-trained networks profit from the patches by using them as a guidance. An adjustment of the probability that a bounding box contains a patch during adversarial training to only $\pi=0.05$ instead of $\pi=0.25$ improves the unpatched performance while maintaining the performance on the prime patches (see Table 5).

In comparison to the results of Table 2, the corresponding mAP differences between the networks differ. The best performance, when no patches or grayscale patches are present, is given by the unpatched network. When attacked with prime patches, both, the multipatched network and the autoencoder network surpass the remaining networks. The PCA networks (32, 64, 128) are on par with the single-patched network, when attacked with prime patches, yet, they

Table 2: Mean average precision for the testset of the *INRIA Person* dataset. The model first was trained on the train data and later attacked with the given set of patches. While the YOLOv7 model has not seen any patches during the training, the other models had a 25 percent chance, that a bounding box contained a patch during training. The patch was either a single predefined patch, a random patch from the patch set or a sampled patch with the PCA or an autoencoder method.

	No Patches (n=1)		Grayscaled (n=11)		Prime Patches (n=375)	
Patch Mode	mAP 0.5 ↑	mAP 0.5:0.95 ↑	mAP 0.5 ↑	mAP 0.5:0.95 ↑	mAP 0.5 ↑	mAP 0.5:0.95 ↑
None	0.80	0.66	0.61 ± 0.09	0.46 ± 0.12	0.71 ± 0.04	0.57 ± 0.04
Single-patched	0.85	0.71	0.71 ± 0.06	0.57 ± 0.08	0.89 ± 0.03	0.75 ± 0.02
Multi-patched	0.84	0.70	0.71 ± 0.07	0.57 ± 0.08	0.89 ± 0.02	0.76 ± 0.02
PCA (16)	0.85	0.72	0.69 ± 0.07	0.56 ± 0.08	0.86 ± 0.02	0.72 ± 0.03
PCA (32)	0.82	0.69	0.68 ± 0.07	0.53 ± 0.08	0.85 ± 0.02	0.71 ± 0.02
PCA (64)	0.85	0.70	$\boldsymbol{0.73 \pm 0.06}$	$\boldsymbol{0.59 \pm 0.06}$	0.88 ± 0.02	0.75 ± 0.02
PCA (128)	0.85	0.70	0.72 ± 0.06	0.59 ± 0.07	$\boldsymbol{0.90 \pm 0.02}$	$\boldsymbol{0.76 \pm 0.02}$
AE	0.84	0.70	0.72 ± 0.06	0.59 ± 0.07	0.87 ± 0.02	0.75 ± 0.02
CVAE	0.84	0.70	0.70 ± 0.08	0.56 ± 0.10	0.87 ± 0.02	0.75 ± 0.02

Table 3: Mean average precision for the testset of the *INRIA Person* dataset. The model first was trained on the crowdhuman train data and later attacked with the given set of patches.

	No Patches (n=1)		Grayscaled (n=11)		Prime Patches (n=375)	
Patch Mode	mAP 0.5 ↑	mAP 0.5:0.95 ↑	mAP 0.5 ↑	mAP 0.5:0.95 ↑	mAP 0.5 ↑	mAP 0.5:0.95 ↑
None	0.95	0.91	0.85 ± 0.01	$\boldsymbol{0.78 \pm 0.02}$	0.84 ± 0.03	0.75 ± 0.05
Single-patched	0.89	0.79	0.76 ± 0.04	0.66 ± 0.04	0.93 ± 0.04	0.84 ± 0.05
Multi-patched	0.84	0.74	0.72 ± 0.02	0.62 ± 0.02	0.95 ± 0.04	$\boldsymbol{0.88 \pm 0.05}$
PCA (16)	0.87	0.78	0.66 ± 0.05	0.56 ± 0.05	0.90 ± 0.04	0.80 ± 0.05
PCA (32)	0.88	0.78	0.71 ± 0.04	0.60 ± 0.04	0.94 ± 0.05	0.85 ± 0.06
PCA (64)	0.83	0.75	0.69 ± 0.03	0.60 ± 0.02	0.93 ± 0.08	0.86 ± 0.09
PCA (128)	0.84	0.76	0.70 ± 0.03	0.61 ± 0.03	0.93 ± 0.07	0.86 ± 0.08
AE	0.88	0.76	0.77 ± 0.05	0.65 ± 0.06	$\boldsymbol{0.95 \pm 0.02}$	0.84 ± 0.02
CVAE	0.88	0.77	0.66 ± 0.06	0.53 ± 0.07	0.92 ± 0.05	0.84 ± 0.06

perform worse when no patches or grayscale patches are present. The lowest overall performance is given by the PCA (16) network, followed by the CVAE network.

Due to computational intensity, the worth of training an auto encoder is questionable. Especially, since a similar performance can be achieved with a single patch.

5 Conclusion

This paper provides an in-depth analysis of adversarial patches, used to fool object detectors. To be more specific, a set of so-called prime patches to evade a YOLOv7 based person detector is analyzed. A qualitative insight into the activations of the backbone network is given, when the detector is attacked with these adversarial patches. The prime patches themselves, are processed by three dimensionality reduction methods, and the mAP drop of their reconstructions is measured. Furthermore, the resulting manifolds of the dimensionality reduction methods are sampled and used in adversarial training. The results indicate that the training of more sophisticated manifold learning methods does not provide a significant better or more varying way to sample adversarial patches. The inclusion of a small set of prime patches or sampled patches using a PCA is sufficient. Moreover, relying on a diverse set of sampled patches using a learned representation results only in a small improvement compared to naive adversarial training.

The results also show that the three investigated dimensionality reduction methods are able to capture some of the necessary features that are required to fool an object detector. This is a further indication that the manifold assumption applies to adversarial patches. Future work should therefore check other manifold learning methods and use the resulting knowledge to enhance protection mechanisms against this kind of attack.

Appendix A Additional Data

ID	Epochs	LR-Scheduler	Resize range	Rotation
A	125	StepLR	[0.5, 0.75]	45
В	100	StepLR	[0.75, 1.0]	45
C	100	CosineAnnealingLR	[0.75, 1.0]	30
D	125	StepLR	[0.5, 0.75]	30
E	100	StepLR	[0.75, 1.0]	30

Table 4: Different parameterization for the patch generation. The resize range is the range of the scaling factor, relatively to the bounding box [2].

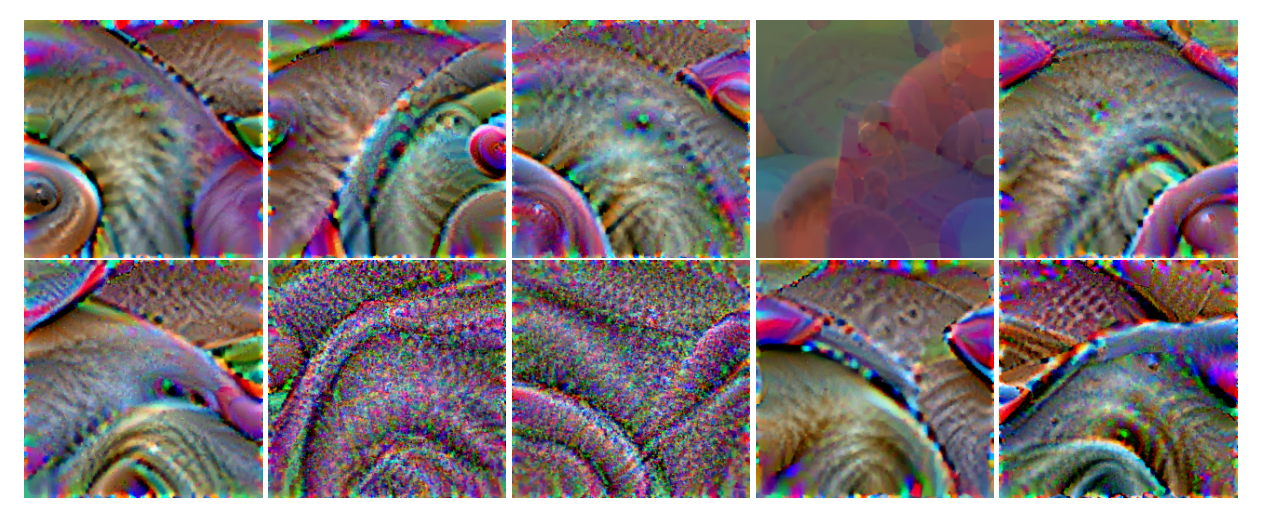


Figure 6: The 10 randomly predefined prime patches used in the training for the multi-patched network.

Table 5: Mean average precision for the testset of the *INRIA Person* dataset. The model first was trained on the crowdhuman train data with $\pi=0.05$ and later attacked with the given set of patches.

	No Patches (n=1)		Grayscaled (n=11)		Prime Patches (n=375)	
Patch Mode	mAP 0.5 ↑	mAP 0.5:0.95 ↑	mAP 0.5 ↑	mAP 0.5:0.95 ↑	mAP 0.5 ↑	mAP 0.5:0.95 ↑
None	0.94	0.89	0.82 ± 0.01	0.74 ± 0.02	0.83 ± 0.04	0.71 ± 0.07
Single-patched	0.92	0.86	0.83 ± 0.01	0.74 ± 0.02	0.92 ± 0.02	0.85 ± 0.03
Multi-patched	0.94	0.88	0.83 ± 0.01	0.74 ± 0.01	$\boldsymbol{0.95 \pm 0.02}$	$\boldsymbol{0.89 \pm 0.02}$
PCA (16)	0.91	0.81	0.77 ± 0.03	0.66 ± 0.03	0.92 ± 0.03	0.83 ± 0.04
PCA (32)	0.93	0.87	0.82 ± 0.01	0.74 ± 0.01	0.93 ± 0.03	0.86 ± 0.04
PCA (64)	0.93	0.87	0.82 ± 0.01	0.72 ± 0.01	0.93 ± 0.04	0.86 ± 0.05
PCA (128)	0.94	0.88	0.80 ± 0.01	0.72 ± 0.02	0.93 ± 0.04	0.85 ± 0.05
AE	0.93	0.87	$\boldsymbol{0.85 \pm 0.01}$	$\boldsymbol{0.77 \pm 0.01}$	0.95 ± 0.02	0.88 ± 0.02
CVAE	0.93	0.87	0.81 ± 0.01	0.73 ± 0.01	0.93 ± 0.03	0.86 ± 0.04

Acknowledgements

This work was developed in Fraunhofer Cluster of Excellence "Cognitive Internet Technologies".

References

- [1] Charles Fefferman, Sanjoy Mitter, and Hariharan Narayanan. Testing the manifold hypothesis. *Journal of the American Mathematical Society*, 29(4):983–1049, 2016.
- [2] Jens Bayer, Stefan Becker, David Münch, and Michael Arens. Eigenpatches—adversarial patches from principal components. In *Advances in Visual Computing*, pages 274–284, Cham, 2023. Springer Nature Switzerland.
- [3] Chien-Yao Wang, Alexey Bochkovskiy, and Hong-Yuan Mark Liao. Yolov7: Trainable bag-of-freebies sets new state-of-the-art for real-time object detectors. In *CVPR*, pages 7464–7475, 2023.
- [4] Bilel Tarchoun, Anouar Ben Khalifa, Mohamed Ali Mahjoub, and Nael Abu-ghazaleh. Jedi: Entropy-based Localization and Removal of Adversarial Patches. In *CVPR*, pages 4087–4095, 2023.
- [5] Florian Tramèr, Nicolas Papernot, Ian Goodfellow, Dan Boneh, and Patrick McDaniel. The Space of Transferable Adversarial Examples. In *arXiv Prepr.*, pages 1–15, 2017.
- [6] Zhi Ming Wang, Meng Ting Gu, and Jia Hui Hou. Sample Based Fast Adversarial Attack Method. *Neural Process. Lett.*, 50(3):2731–2744, 2019.
- [7] Ruoxi Shi, Borui Yang, Yangzhou Jiang, Chenglong Zhao, and Bingbing Ni. Energy Attack: On Transferring Adversarial Examples. In *arXiv Prepr.*, 2021.
- [8] Elvis Dohmatob, Chuan Guo, and Morgane Goibert. Origins of low-dimensional adversarial perturbations. In Francisco Ruiz, Jennifer Dy, and Jan-Willem van de Meent, editors, AISTATS, pages 9221–9237, 25–27 Apr 2023.
- [9] Ali Shafahi, Ronny Huang, Christoph Studer, Soheil Feizi, and Tom Goldstein. Are adversarial examples inevitable? *ICLR*, 2019.
- [10] Juanjuan Weng, Zhiming Luo, Dazhen Lin, Shaozi Li, and Zhun Zhong. Boosting Adversarial Transferability via Fusing Logits of Top-1 Decomposed Feature. *arXiv Prepr.*, may 2023.
- [11] Washington Garcia, Pin-Yu Chen, Hamilton Scott Clouse, Somesh Jha, and Kevin R.B. Butler. Less is more: Dimension reduction finds on-manifold adversarial examples in hard-label attacks. In *SaTML*, pages 254–270, 2023.
- [12] Naveed Akhtar and Ajmal Mian. Threat of adversarial attacks on deep learning in computer vision: A survey. *IEEE Access*, 6:14410–14430, 2018.
- [13] Anirban Chakraborty, Manaar Alam, Vishal Dey, Anupam Chattopadhyay, and Debdeep Mukhopadhyay. A survey on adversarial attacks and defences. *CAAI Trans. Intell. Technol.*, 6(1):25–45, 2021.
- [14] Cato Pauling, Michael Gimson, Muhammed Qaid, Ahmad Kida, and Basel Halak. A Tutorial on Adversarial Learning Attacks and Countermeasures. In *arXiv Prepr.*, 2022.
- [15] Shunxin Wang, Raymond Veldhuis, and Nicola Strisciuglio. The Robustness of Computer Vision Models against Common Corruptions: a Survey. *arXiv Prepr.*, pages 1–23, may 2023.
- [16] Charles Godfrey, Henry Kvinge, Elise Bishoff, Myles Mckay, Davis Brown, Tim Doster, and Eleanor Byler. How many dimensions are required to find an adversarial example? In *CVPRW*, pages 2353–2360, 2023.
- [17] L. Sirovich and M. Kirby. Low-dimensional procedure for the characterization of human faces. *Journal of the Optical Society of America A*, 4(3):519, 1987.
- [18] Kamal Berahmand, Fatemeh Daneshfar, Elaheh Sadat Salehi, Yuefeng Li, and Yue Xu. Autoencoders and their applications in machine learning: a survey. *Artificial Intelligence Review*, 57(2):28, 2024.
- [19] Kihyuk Sohn, Xinchen Yan, and Honglak Lee. Learning structured output representation using deep conditional generative models. *Advances in Neural Information Processing Systems*, 2015-January:3483–3491, 2015.
- [20] Diederik P. Kingma and Max Welling. Auto-encoding variational bayes. In Yoshua Bengio and Yann LeCun, editors, 2nd International Conference on Learning Representations, ICLR 2014, Banff, AB, Canada, April 14-16, 2014, Conference Track Proceedings, 2014.
- [21] N. Dalal and B. Triggs. Histograms of Oriented Gradients for Human Detection. In *CVPR*, volume 1, pages 886–893, 2005.
- [22] Shuai Shao, Zijian Zhao, Boxun Li, Tete Xiao, Gang Yu, Xiangyu Zhang, and Jian Sun. CrowdHuman: A Benchmark for Detecting Human in a Crowd. pages 1–9, 2018.
- [23] Ilya Loshchilov and Frank Hutter. Decoupled weight decay regularization. ICLR, 2019.